# Use of the Richtmyer-Meshkov Instability to Infer Yield Stress at High-Energy Densities

Guy Dimonte, G. Terrones, F. J. Cherne, T. C. Germann, V. Dupont, K. Kadau, W. T. Buttler, D. M. Oro, C. Morris, and D. L. Preston

*Los Alamos National Laboratory, Los Alamos, New Mexico 87545, USA*

(Received 15 July 2011; published 23 December 2011)

We use the Richtmyer-Meshkov instability (RMI) at a metal-gas interface to infer the metal's yield stress ($Y$) under shock loading and release. We first model how $Y$ stabilizes the RMI using hydrodynamics simulations with a perfectly plastic constitutive relation for copper (Cu). The model is then tested with molecular dynamics (MD) of crystalline Cu by comparing the inferred $Y$ from RMI simulations with direct stress-strain calculations, both with MD at the same conditions. Finally, new RMI experiments with solid Cu validate our simulation-based model and infer $Y \sim 0.47$ GPa for a 36 GPa shock.

DOI: 10.1103/PhysRevLett.107.264502 PACS numbers: 47.20.Bp

In the Richtmyer-Meshkov instability (RMI), a shock amplifies perturbations at material interfaces at a rate that depends on the material properties. In melted materials, the RMI is fluidlike and grows linearly in time until nonlinearities reduce the growth rate in an asymmetric manner ([1] and references therein). In materials with strength (i.e., yield stress $Y \neq 0$), the RMI growth is arrested and stabilized at an amplitude $h^{\max} \propto 1/Y$. Piriz *et al.* [2] (P08) used two-dimensional simulations of perturbations at a vacuum-metal interface (Atwood number $A = +1$) to obtain a relation between $h^{\max}$, $Y$, and RMI dynamical parameters. Piriz *et al.* [3] then suggested using the relation to infer an effective $Y$ at high-energy density, but it has not been tested experimentally nor with real materials. We are studying the complementary metal-gas system ($A \sim -1$) in which shocks produce ejecta [4–6] in order to develop a RMI-based model for the amount and velocity of ejecta both below and above melt conditions.

Here, we begin our model development by studying the RMI in copper (Cu) with $Y \neq 0$ in three steps. First, we use full hydrodynamic simulations (HS) of an ideal Cu-gas system to obtain a relation between $h^{\max}$, $Y$, and RMI dynamical quantities. With $A \sim -1$, we find it necessary to describe the RMI in the nonlinear regime and with asymmetric growth beyond that done in P08. For clarity, the Cu remains solid with an assigned $Y$ using a perfectly plastic constitutive relation. Second, we test our model self-consistently using molecular dynamics (MD) simulations by comparing direct measurements of $Y$ with those inferred from MD-RMI simulations. Both are done with MD of single crystalline Cu under similar conditions and realistic material properties. Third, we apply our model to new RMI experiments with polycrystalline Cu below melt to infer a $Y$ that compares favorably with the prediction in Ref. [7]. These results are important for describing the hydrodynamics and ejecta in shock-driven applications involving metals.

We first study the strength suppression of the RMI using HS of an idealized Cu-gas system with PAGOSA [8]. PAGOSA is an Eulerian finite-difference multimaterial hydrodynamics code with a variety of thermodynamic, material strength, and high-explosive (HE) models. In a configuration like Fig. 1 of Ref. [1], we launch a shock in the Cu ($A$) toward a perturbed interface with a perfect gas ($B$). The Cu has a density $\rho_A = 8.9$ g/cm$^3$ and remains a solid with an assigned constant $Y$. The gas has little influence due to its low density $\rho_B = 1.22$ mg/cm$^3$ $\ll \rho_A$ [$A = (\rho_B - \rho_A)/(\rho_B + \rho_A) \sim -1$] and is given a specific heat ratio $\gamma_B = 5/3$. The initial shock satisfies the Cu Hugoniot relation $W_i = 3.94$ km/s $+ 1.489u_3$, where $W_i$ is the incident shock speed and $u_3$ is the trailing particle speed. In characterizing the machined surfaces [5], we find that they are mainly 2D single-mode perturbations. Thus, our HS are 2D and use one wavelength $\lambda \equiv 2\pi/k = 4.3$ cm with 86 zones/$\lambda$ for numerical convergence, where $k$ is the wave number. The initial perturbation has an amplitude $h_0^-$ prior to the shock arrival and $h_0^+ = h_0^-(1 - U/W_i)$ after the shock transit, where $U$ is the acquired interface speed.

PAGOSA simulations with $Y = 0.5$ GPa are exemplified in Fig. 1 in scaled units (defined below) for 4 values of $kh_0^-$. For brevity, the images depict only the interfacial regions with Cu in yellow and gas in black. Each case uses a drive pressure of 160 GPa to produce a right-moving shock with $u_3 = 2.5$ km/s, $W_i = 7.64$ km/s, and $U = 5.26$ km/s, and, on release, a Cu density of 8.3 g/cm$^3$ and temperature $T \sim 1300$ K. The RMI growth rate increases with $kh_0^-$ and is negative for $A \sim -1$ [9]. Thus, the perturbation inverts phase after the shock compression, and then grows asymmetrically due to $A = -1$ and at a reduced rate due to $Y$. To understand this complex evolution, we first clarify our geometry. As shown in the first image, the initial perturbation is taken to be $Z(t = 0^-) = h_0^- \cos(kx)$ relative to a flat interface ($Z \equiv 0$) with $Z > 0$ to the right. The shock first compresses the perturbation to $h_0^+/h_0^- \sim 0.33$ with the same phase since $U < W_i$. The perturbation then grows negatively so that the depression in the center ($kx = \pi$) becomes a protrusion that we call a

 

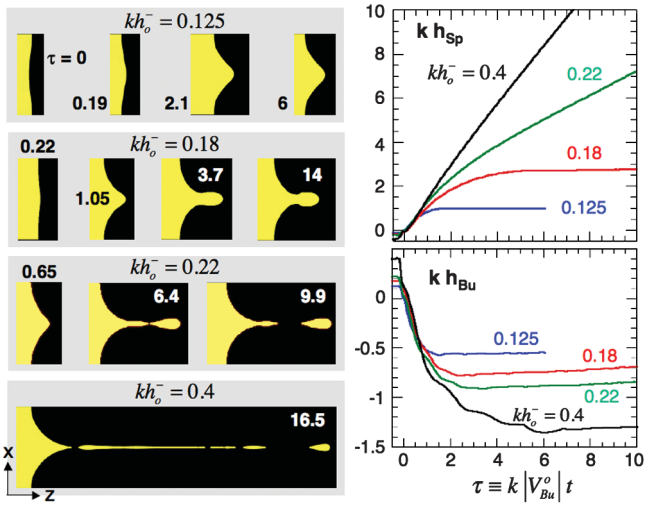


FIG. 1 (color). RMI simulations using PAGOSA with Cu (yellow) and gas (black) with $Y = 0.5$ GPa and $u_3 = 2.5$ km/s.

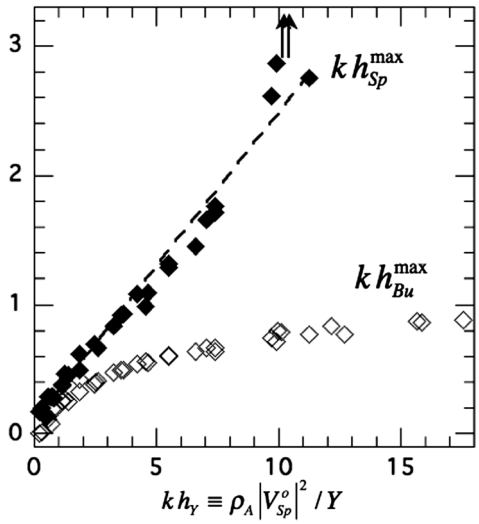


FIG. 2. Scaled saturation amplitudes for spikes (solid symbols) and bubbles (open symbols) from PAGOSA simulations versus RMI strength parameter.

spike of heavy material. The initial protrusions at $kx = 0$ and $2\pi$ become depressions that we call bubbles of light fluid. Such a slow phase inversion is predicted by linear theory [9] and observed experimentally [10] for $A < 0$. In our convention, the scaled spike (bubble) amplitude $kh_{sp}$ ($kh_{bu}$) starts negative (positive) and "grows" in the opposite direction. To distinguish bubbles and spikes, we perform separate simulations with flat interfaces for $Z(t)$. Time is scaled by the peak bubble growth rate $V_{bu}^0 \equiv \max(dh_{bu}/dt)$, namely, as $\tau \equiv k|V_{bu}^0|t$, because we find that $V_{bu}^0$ agrees with the Meyer-Blewett [11] growth rate $V_{MB} = -Uk(h_0^- + h_0^+)/2$ for $A = -1$ and $kh_0^- < 0.5$. Conversely, the harmonics "accelerate" the spikes in the fluid regime to a velocity $V_{sp}^0 \equiv \max(dh_{sp}/dt) \Rightarrow V_{bu}^0\sqrt{3(kh_0^- + 1)/(3kh_0^- + 1)}$ [1,12,13].

Figure 1 shows that bubbles and spikes evolve quite differently for $A \sim -1$ and $Y \neq 0$. The bubbles always saturate but the amplitude increases with $kh_0^-$ since it determines the RMI growth rate. The spikes saturate and remain contiguous with the bulk Cu only for $kh_0^- \leq 0.18$. For $kh_0^- = 0.22$, the spikes detach from the bulk Cu but without further change in morphology. For $kh_0^- = 0.4$, they continue to elongate and eventually disintegrate into particles. These results suggest an ejecta transition in which the saturated bubbles (spikes) determine the amount (velocity) of the ejecta, even for unmelted materials.

We generalized the results in Fig. 1 using PAGOSA simulations with different values of $W_i$, $kh_0^-$, and $Y$. The results are summarized in Fig. 2 by plotting the scaled saturation amplitudes $|kh_{bu}^{max}|$ and $|kh_{sp}^{max}|$ versus the RMI strength parameter

$$kh_Y \equiv \frac{\rho_A}{Y}|V_{sp}^0|^2. \tag{1}$$

The spikes are well described by the least-squares fit (dashed line in Fig. 2)

$$|kh_{sp}^{max}| = 0.08 + 0.24\ kh_Y. \tag{2}$$

Our coefficient of 0.24 for $A = -1$ is smaller than the 0.29 of P08 for $A = +1$, which is reasonable since RMI growth rates differ with the sign of $A$. Our intercept of 0.08 may be related to the amplitude $\xi_0$ defined by P08 to be where strength becomes important. Since both are small and somewhat ambiguous, we estimate an average RMI (perfectly plastic) yield from Eq. (2) to be

$$Y_{RMI} \sim 0.24\rho_A \frac{|V_{sp}^0|^2}{kh_{sp}^{max}} \tag{3}$$

for $A \sim -1$, with an uncertainty of 10%–20% for observations near $kh_{sp}^{max} \sim 1$. We focus Eqs. (1)–(3) on spikes because they grow faster and to larger amplitudes than bubbles for $|A| \sim 1$, as seen in Ref. [1] and Fig. 1. This makes spikes easier to observe, as shown below. In addition, the spikes saturate at an amplitude that increases simply with $kh_Y$ and they exhibit a dramatic transition to unbounded secular growth when $kh_Y \geq 10 \pm 1$. The uncertainty arises since we observe 3 cases with $kh_Y \sim$ 9.5–11.5 (diamonds) where the spikes saturate and 2 cases at $kh_Y \sim 10$ (arrows) that grow indefinitely. In contrast, the bubbles saturate at smaller amplitudes and for all $kh_Y$. Even in the fluid regime ($kh_Y \Rightarrow \infty$), the bubble velocity decays as $1/kt$ asymptotically. By mass conservation, this asymmetric growth causes the spikes to become very narrow and eventually disintegrate into ejecta particles. This will form the basis for a future ejecta source model.

We now test our RMI strength-suppression model with MD by comparing $Y_{RMI}$ from MD-RMI simulations with a direct calculation of $Y$, both with the SPASM code [14] at similar $T$ and strain rate (SR). MD can describe small-scale mixing and material damage from void growth in an *ab initio* manner because they describe atomic interactions.

We use an embedded atom method [15] for Cu with a 0.5 nm potential cutoff radius. The domain is 2.6 nm deep to reduce edge effects and 2D in $X$-$Z$ with $\lambda =$ 257 nm and (50–60) $\times 10^6$ atoms in a fcc lattice next to a vacuum ($A = -1$). Figure 3 shows MD-RMI results for an 83 GPa incident shock with $u_3 = 1.5$ km/s, $W_i =$ 6 km/s, and $U = 3$ km/s. On release, the Cu at $\sim$8.7 g/cm$^3$ and $T \sim 1003$ K remains below the melt temperature (1350 K). The initial perturbations at $kh_0^- = 1$ are first compressed to $kh_0^+ \sim 0.5$ as expected. They then grow with $V_{\rm bu}^0 \sim -0.44 \pm 0.08$ km/s and $V_{\rm sp}^0 \sim 0.6 \pm 0.1$ km/s. Both are smaller than $V_{\rm MB} \sim 2.25$ km/s due to nonlinearities [1] and strength. The strength-induced saturation amplitudes $|kh_{\rm bu}^{\rm max}| \sim kh_{\rm sp}^{\rm max} \sim 0.67$ are similar because $kh_Y$ is small, but the asymmetry increases with $kh_Y$ in our MD-RMI simulations, similar to Figs. 1 and 2. Inserting $kh_{\rm sp}^{\rm max}$ and $V_{\rm sp}^0$ into Eq. (3), we obtain $Y_{\rm RMI} = 1.1 \pm 0.3$ GPa. We believe the differences between Figs. 1 and 3 occur because $kh_Y \sim 2.7$ is small compared to 4.6, 11.3, 17.6, and 63.4 for the four cases in Fig. 1, and the yield curve is more realistic.

The stress-strain curve is calculated directly with MD, as shown in Fig. 4 for the conditions in Fig. 3. A Cu crystal ($36 \times 289 \times 2$ nm) is prepared at $T = 1003$ K and the resistance force (stress) is measured while the sample is sheared at an SR $\sim$ ns$^{-1}$ (SR varies from 0 to $kV_{\rm sp} \sim$ 10 ns$^{-1}$ in our MD-RMI simulations). In Fig. 4, $Y$ varies in the range of 1.2–1.5 GPa for strains $<$0.2 and decreases to 0.65 GPa at the peak strain $|kh_{\rm sp}^{\rm max}| \sim 0.7$ in Fig. 3 due to plastic work since $T$ increases by $\sim$200 K. For strains of 0–0.7, we obtain an average $Y = 0.95 \pm 0.3$ GPa which is consistent with $Y_{\rm RMI}$ from our MD-RMI simulations. These values are also consistent with the peak $Y \sim$ 1.4 GPa obtained in Refs. [7,16] for our conditions.

Finally, we apply our model to Cu experiments [6] driven by HE and diagnosed with proton radiography and laser Doppler velocimetry (LDV), as shown in Fig. 5. The HE generates a 36 GPa shock in a 6 mm thick Cu plate with $W_i \sim 5$ km/s and $U = 1.46$ km/s. $U$ is measured directly with LDV on 3 flat regions (black arrows) while $W_i$ and $T \leq 500$ K are inferred from Cu Hugoniot relations. There are 4 sets of initial perturbations with $\lambda = 0.55$ mm and $kh_0^- = 0.75$, 0.12, 0.35, and 1.5 to span $kh_Y$. The proton radiography images show the perturbations with $kh_0^- \leq 0.35$ being stabilized by $Y$, whereas those with $kh_0^- \geq 0.75$ exceed the ejecta transition and grow secularly. To infer $Y_{\rm RMI}$, we first subtract the LDV velocities [inset (a)] in front of the $kh_0^- = 0.35$ perturbation (red solid line) for $V_{\rm sp} + U$ and the flats (black line) for $U$ to obtain the net spike growth rate (red dashed line) $V_{\rm sp}$. (This parallels our simulations with and without perturbations to discern bubbles and spikes.) The peak spike growth rate $V_{\rm sp}^0 \sim 0.59 \pm 0.02$ km/s is 40% larger than $|V_{\rm MB}| \sim 0.43$ km/s perhaps due to the spike acceleration by the harmonics [1,12]. We then integrate $kV_{\rm sp}$ [inset (b)] to obtain the net scaled spike growth $kh_{\rm sp}^{\rm max} - kh_0^+ \sim 1.85$ relative to its initial postshock initial amplitude $kh_0^+ \sim -0.29$. (Negative due to opposite phase as in Figs. 1 and 2.) Thus, the saturated spike amplitude is $kh_{\rm sp}^{\rm max} \sim 1.56$. Inserting $V_{\rm sp}^0$ and $kh_{\rm sp}^{\rm max}$ into Eq. (3), we obtain an average $Y_{\rm RMI}$ of 0.47 $\pm$ 0.1 GPa over a strain of 0 to $kh_{\rm sp}^{\rm max}$. This agrees with the shear stress $Y \sim 0.57$ and 0.5 GPa from Refs. [7,17], respectively, for SR $\sim$ 1–10 $\mu$s$^{-1}$. Similarly, we analyzed the case for $kh_0^- = 0.12$ where LDV gives a peak $V_{\rm sp}^0 \sim 0.13 \pm 0.02$ km/s $\sim 0.85|V_{\rm MB}|$ and $kh_{\rm sp}^{\rm max} - kh_0^+ \sim 0.17 \pm 0.03$ upon integration. With $kh_0^+ \sim -0.09$, we insert $kh_{\rm sp}^{\rm max} \sim 0.08 \pm 0.03$ and $V_{\rm sp}^0$ into Eq. (3) to obtain $Y_{\rm RM} \sim 0.4 \pm 0.2$ GPa. This is consistent with the result at $kh_0^- = 0.35$, but the relative uncertainty is larger due to the weaker RMI response at smaller amplitude. Thus, the precision for $Y_{\rm RM}$ can be improved by varying $kh_0^-$ in finer increments to obtain $|kh_0^+| \ll kh_{\rm sp}^{\rm max} < 2.5$ and $V_{\rm sp}^0 \gg 0.02$ km/s (LDV uncertainty).

In summary, we developed a model for the strength suppression of the RMI that can be used to infer yield

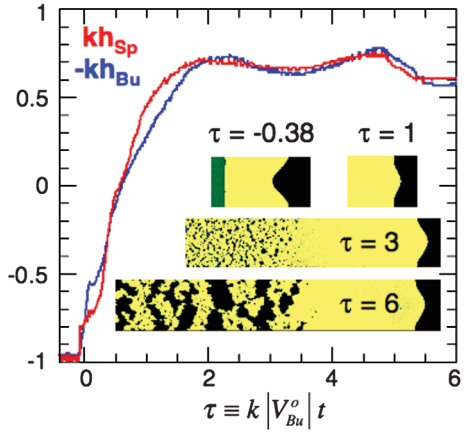


FIG. 3 (color). Scaled amplitudes and images from SPASM simulations for $u_3 = 1.5$ km/s and $kh_0^- = 1$.

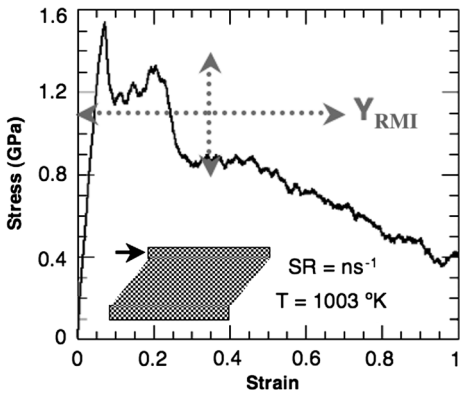


FIG. 4. Stress-strain calculations with SPASM for Cu conditions in Fig. 3 at $T \sim 1000$ K.

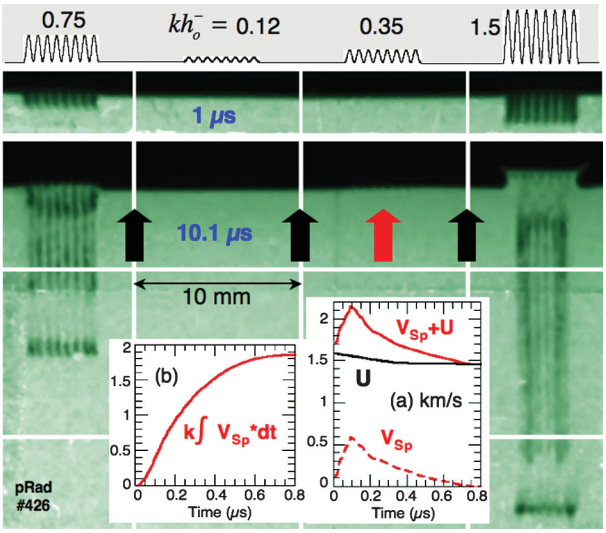


FIG. 5 (color). RMI experiment with Cu. Top profile shows 4 initial machined perturbations separated by flat regions. Proton radiography (pRAD) images taken at $t = 1$ $\mu$s (top) and 10.1 $\mu$s (bottom) relative to shock breakout. LDV probes measure $U$ on flats (black arrows) and $U + V_{sp}$ in front of perturbations (red arrow) with $kh_0^- = 0.35$. Inset (a) measured LDV velocities (solid lines) and spike growth rate $V_{sp}$ (dashed line) in km/s. Inset (b) integral of $kV_{sp}$ for net spike growth.

under shock loading. The model is based on ideal hydrodynamic simulations and corroborated by MD simulations that compare the RMI inferred yield with direct yield measurements under the same conditions. The model is able to infer the yield of copper in an explosively driven experiment that agrees with previous results. We plan to refine the model and experimental techniques in order to characterize different materials under various shock conditions below and above the ejecta transition. In particular, we note that LDV probes provide a sensitive measure of the RMI, but they apply better to the spikes in front than the bubbles in back. This motivated our formulation of Eqs. (1)–(3) in terms of spikes, especially since bubbles saturate at smaller amplitudes with a more complex dependence on $kh_Y$.

We thank A. R. Piriz and K. O. Mikaelian for useful discussions and D. Tupa for fielding LDV. This work was performed for the U.S. Department of Energy by Los Alamos National Laboratory under Contract No. DE-AC52-06NA2-5396.

[1] Guy Dimonte and P. Ramaprabhu, Phys. Fluids **22**, 014104 (2010).
[2] A. R. Piriz, J. J. Lopez Cela, N. A. Tahir, and D. H. H. Hoffmann, Phys. Rev. E **78**, 56401 (2008).
[3] A. R. Piriz, J. J. Lopez Cela, and N. A. Tahir, Nucl. Instrum. Methods Phys. Res., Sect. A **606**, 139 (2009).
[4] J. R. Asay, L. P. Mix and F. C. Perry, Appl. Phys. Lett. **29**, 284 (1976).
[5] W. S. Vogan *et al.*, J. Appl. Phys. **98**, 113508 (2005); Zellner *et al.*, J. Appl. Phys. **103**, 123502 (2008).
[6] W. T. Buttler *et al.* LANL Report No. LAUR-11-03785, 2011 (to be published).
[7] D. L. Preston, D. L. Tonks, and D. C. Wallace, J. Appl. Phys. **93**, 211 (2003).
[8] W. N. Weseloh, S. P. Clancy, and J. W. Painter, Los Alamos National Laboratory, Report No. LAUR-14425-M, 2010.
[9] G. Fraley, Phys. Fluids **29**, 376 (1986); J. G. Wouchuck, Phys. Plasmas **8**, 2890 (2001).
[10] Guy Dimonte *et al.*, Phys. Plasmas **3**, 614 (1996).
[11] K. M. Meyer and P. J. Blewett, Phys. Fluids **15**, 753 (1972).
[12] Q. Zhang, Phys. Rev. Lett. **81**, 3391 (1998).
[13] K. O. Mikaelian, Phys. Rev. E **81**, 16 325 (2010).
[14] D. M. Beazley and P. S. Lomdahl, Parallel Comput. **20**, 173 (1994).
[15] A. F. Voter, Phys. Rev. B **57**, R13 985 (1998).
[16] M. F. Horstemeyer, M. I. Baskes and S. J. Plimpton, Acta Mater. **49**, 4363 (2001).
[17] K. J. Frutschy and R. J. Clifton, J. Mech. Phys. Solids **46**, 1723 (1998).